IEEE Access
Multidisciplinary | Rapid Review | Open Access Journal

Received 17 December 2023, accepted 1 January 2024, date of publication 10 January 2024, date of current version 29 January 2024.

Digital Object Identifier 10.1109/ACCESS.2024.3352085

RESEARCH ARTICLE

Throughput Maximization for RIS-Assisted UAV-Enabled WPCN

JIAYING ZHANG[1], JIE TANG[1], (Senior Member, IEEE), WANMEI FENG[2], XIU YIN ZHANG[1], DANIEL KA CHUN SO[3], (Senior Member, IEEE), KAT-KIT WONG[4], AND JONATHON A. CHAMBERS[5], (Fellow, IEEE)

[1]School of Electronic and Information Engineering, South China University of Technology, Guangzhou 510641, China
[2]College of Electronic Engineering, South China Agricultural University, Guangzhou 510642, China
[3]Department of Electrical and Electronic Engineering, The University of Manchester, M13 9PL Manchester, U.K.
[4]Department of Electronic and Electrical Engineering, University College London, WC1E 6BT London, U.K.
[5]School of Engineering, University of Leicester, LE1 7RH Leicester, U.K.

Corresponding author: Jie Tang (eejtang@scut.edu.cn)

This work was supported by the National Natural Science Foundation of China under Grant 62222105.

ABSTRACT This paper investigates a reconfigurable intelligent surface (RIS)-assisted unmanned aerial vehicle (UAV)-enabled wireless powered communication network (WPCN). In the system, a UAV acts as a hybrid access point (HAP) to charge users in the downlink (DL) and receive messages in the uplink (UL). In particular, the RIS is exploited to significantly enhance the efficiency of both the DL and UL transmission. Our objective is to enhance the minimum throughput among all ground users by jointly optimizing the horizontal location of UAVs, the transmit power of users, transmission time allocation, and passive beamforming vectors at the RIS. To address this problem, we present an alternating optimization-based algorithm with low complexity to decompose the problem into four subproblems and solve them sequentially. In particular, we derive a lower bound of the composite channel gain to tighten the constraints and employ successive convex approximation (SCA) to optimize the horizontal location of the UAV. The transmit power closed-form optimum solutions are then obtained, and the problem of time allocation is reformulated as a linear programming problem. Finally, we optimize the passive beamforming vectors by adopting semi-definite relaxation (SDR). The effectiveness of the algorithm is supported by numerical results, which also demonstrate that the RIS-assisted UAV-enabled WPCN outperforms the traditional WPCN in terms of the minimum throughput.

INDEX TERMS Wireless powered communication network (WPCN), unmanned aerial vehicle (UAV), reconfigurable intelligent surface (RIS), optimal placement, resource allocation.

I. INTRODUCTION

With the arrival of fifth-generation (5G) mobile communication technology, the applications of Internet of Things (IoT) are growing exponentially, including wearable computing, remote health care, smart cities, and intelligent transportation systems [1], [2]. Due to the proliferation of wireless devices using 5G networks, the volume of data is increasing rapidly [3], [4], leading to the degradation of communication quality. Additionally, it is anticipated that future wireless networks will offer many other requirements, including extremely high throughput, minimal delay, and ultra-high reliability, which will pose a big pressure on wireless communication networks [5]. Besides, the compactness and mobility of wireless terminal devices result in the issue of limited battery life [6], which requires periodic battery replacement or recharging. However, frequent battery replacements incur significant maintenance costs and go against the need for green communications. Therefore, ensuring communication quality while enhancing the lifespan of wireless devices has become a critical concern for both academia and industry.

The problem of limited battery lifetime in mobile devices has been resolved by using wireless power transfer (WPT) [7]. In particular, receivers collect energy sent by the transmitters using the far-field radiative characteristics of electromagnetic waves. There are several benefits to

The associate editor coordinating the review of this manuscript and approving it for publication was Yafei Hou.

radio frequency (RF)-enabled wireless power transmission, including large operational range, low-cost manufacture, and effective energy transfer [8]. Wireless powered communication network (WPCN), which combines WPT with wireless information transfer (WIT), is one of the numerous uses that the development of WPT have brought about for communication networks [9]. In particular, a hybrid access point (HAP) uses RF waves in the downlink (DL) to provide energy to ground users, who then utilize the collected energy to broadcast data in the uplink (UL) [10]. As such, terminal devices can transmit information while ensuring a stable energy source; thus avoiding the maintenance cost of regular battery replacement or charging.

On the other hand, numerous technologies have been developed to reconfigure the wireless propagation environments and increase the communication quality, including unmanned aerial vehicle (UAV) communication and reconfigurable intelligent surfaces (RISs). UAVs have gained significant attention by the industry and the academia because of the strengths of high flexibility, independent operations and fast deployment [11]. For example, the locations of HAPs in traditional wireless communication networks are fixed. This leads to a near-far fairness problem, which can be solved by UAVs deployed in the cell edge [12]. Moreover, UAVs can offer fast deployment for special scenarios such as natural disasters and emergency maintenance with low cost [11]. Therefore, UAVs are gradually used in wireless communication scenarios. However, the line-of-sight (LoS) link between the UAV and ground users could be hindered, especially in an urban environment, that can be mitigated by RISs. RIS can modify the wireless channel environments and improve the communication quality [13]. Unlike other technologies applied to wireless networks, RISs do not need energy sources and can be quickly deployed [14]. The deployment of RISs provides wireless communication systems with the ability to reshape the channels. Particularly, wireless transmission environments can be intelligently manipulated by designing the RIS reflective coefficients, which solves challenges such as blind coverage and channel environment deterioration [15].

The combination of UAV and RIS will further enhance the propagation environment and communication quality [16], [17]. It is proven that installing multiple antennas on wireless transceivers significantly improves the communication performance by exploiting the multiplexing gain [18]. However, several antennas may not be suitable to be implemented in UAVs on account of the restrictions of size, weight, and power. Moreover, if we apply multiple antennas to UAVs, the hovering place design of the UAV will couple with the precoding design of multi-antennas, leading to highly non-convex optimization problems [19]. In contrast, RIS can simulate multiple-input multiple-output (MIMO) gain, providing a promising resolution to this challenge [20].

Motivated by the several benefits of the mentioned technologies, researchers have explored ways to integrate RIS, UAV and WPCN. The placement of UAVs and resource allocation are major problems in RIS-assisted UAV-enabled WPCNs. Some previous works have investigated the UAV-enabled WPCNs and RIS-assisted WPCNs under different scenarios. For instance, the authors in [21] aimed to maximize the minimum throughput in UAV-enabled WPCNs, which was transferred into a traveling salesman problem and was solved by the Lagrange dual approach. Furthermore, to increase the stability and dependability of wireless sensor networks in emergency scenarios, the authors in [22] studied the UAV hovering strategy and employed a greedy algorithm to obtain the optimal hovering location of UAVs. Besides, the author in [23] explored two different energy harvesting models, including the linear and the non-linear, and solved the problems by using the concave-convex procedure and successive convex approximation (SCA) respectively. For the case of multiple UAVs, the authors in [24], [25], and [26] studied a multiple UAVs WPCN system, by considering the inference from the non-target cluster.

Unlike the UAV-enabled WPCN, the phase shift matrix design is the crucial problem in a RIS-assisted WPCN. In [27], the authors optimized the resource allocation of a RIS-aided WPCN, in which the triangle inequality is applied to simplify the composite channel gain and a semi-definite program (SDP) is employed to address the phase shifts optimization problem. A self-sustainable RIS-powered WPCN system was examined by the authors in [28] by incorporating the energy consumption of the RIS into the analysis. The authors in [29] studied the RIS-aided WPCN and proposed that dynamic RIS is not needed for the RIS-aided WPCN, simplifying the algorithm. Furthermore, the authors in [30] and [31] studied RIS-aided half-duplex and full-duplex WPCN under three types of RIS beamforming configurations.

A. MAIN CONTRIBUTIONS

The prior works focused on investigating UAV-enabled WPCN or RIS-assisted WPCN to extend the lifespan of devices while ensuring the quality of communication. However, most works investigating UAV-enabled WPCN consider the LoS path channel between the UAV and devices [21], [22], [23], [24], [25], [26], which ignore the impact of the high building in the LoS link. On the other hand, previous works focused on RIS-assisted WPCN consider the users in signal cell and near-far fairness problem will exist [27], [28], [29], [30], [31]. In contrast to [21], [22], [23], [24], [25], [26], [27], [28], [29], [30], and [31], this paper integrates the UAV and RIS in the context of WPCN, in which non-light-of-sight (NLoS) link between the UAV and devices is taken into account. Moreover, fairness problem of devices is solved by employing UAV flying around the cell and maximizing the minimum throughput of all the users instead of the overall system throughput. Particularly, a UAV sends out energy signals to ground users in the DL while users use the collected energy to transmit data to the UAV in the UL.

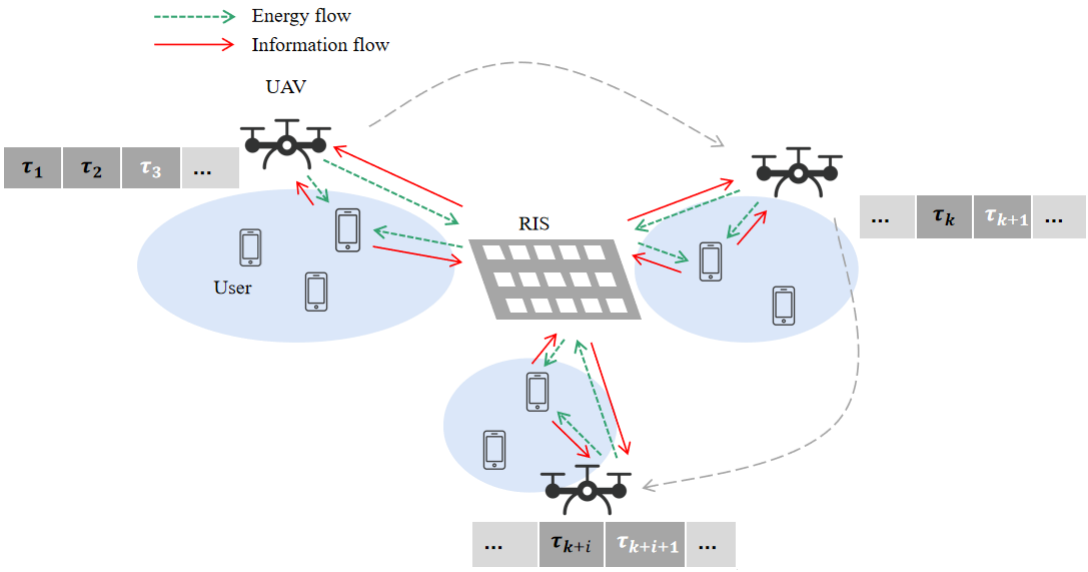

FIGURE 1. A RIS-assisted UAV-enabled WPCN.

A RIS is installed at the tower to enhance the communication efficiency. The following list summarizes the key points of our paper.

- To satisfy the high data rate demand and solve the network lifetime problem, we propose a RIS-assisted UAV-enabled WPCN. Based on this framework, we formulate a minimum throughput maximization problem by jointly optimizing the 2D hovering location of the UAV, the transmit power of users, transmission time allocation and RIS passive beamforming subject to an energy constraint. However, the minimum throughput maximization problem, with its non-convexity, is difficult to solve because of the coupled 2D position of the UAV and passive beamforming of the RIS.
- To tackle this problem, we develop a low-complexity algorithm based on alternating optimization in which the primary issue is divided into four subproblems and solved alternatively. First, we establish the minimum boundary of the composite channels and tighten the constraints of the formulated problem. Then, in order to determine the optimal 2D hovering location of UAV, we provide a method based on SCA. We obtain the closed-form solution of the transmit power and convert the time allocation problem into a linear programming problem after obtaining the horizontal placement of the UAV. Finally, we optimize the reflective coefficients of RIS by using semi-definite relaxation (SDR) method.
- Numerical results support that the effectiveness of our proposed algorithm for the RIS-assisted UAV-enabled WPCN. We also conduct a comparative analysis between our proposed algorithm and several benchmark algorithms to demonstrate the advantages of our approach.

II. SYSTEM MODEL AND PROBLEM FORMULATION

We consider a RIS-assisted UAV-enabled WPCN with K users, as depicted in Figure 1, in which a RIS is mounted at the top of a towering building to aid wireless communication systems. The entire region is split into S service areas according to the distribution of ground users. Both the UAV and ground users are equipped with a single-antenna. The RIS is made up of $M > 1$ reflective units. The total number of ground users is denoted as K. We assume that users in each service is relatively fixed and the position of the κ-th ground user can be represented as $\boldsymbol{z}_\kappa = (x_\kappa, y_\kappa, 0)$, $\kappa \in \mathcal{K} \triangleq \{1, \ldots, K\}$, while the horizontal coordinate of the κ-th user is specified as $\boldsymbol{w}_\kappa = (x_\kappa, y_\kappa)$. The UAV in $s \in \mathcal{S} \triangleq \{1, \ldots, S\}$ service area is fixed at h to ensure that the coverage of UAV remains unchanged. The horizontal location of UAV is given by $\boldsymbol{w}_{s,u} = (x_{s,u}, y_{s,u})$, the adjustment of which has less requirement on flight stability compared with the height. The RIS is mounted on a building's wall at height H and its horizontal placement is given by $\boldsymbol{w}_R = (x_R, y_R)$. Consequently, $d_{s,\kappa}^{UG} = \sqrt{\|\boldsymbol{w}_{s,u} - \boldsymbol{w}_\kappa\|^2 + h^2}$ denotes the distance between the UAV and user $\kappa \in \mathcal{K}$, and $d_s^{UR} = \sqrt{\|\boldsymbol{w}_{s,u} - \boldsymbol{w}_R\|^2 + (h-H)^2}$ indicates the distance between the UAV and the RIS. Moreover, $d_\kappa^{RG} = \sqrt{\|\boldsymbol{w}_R - \boldsymbol{w}_\kappa\|^2 + H^2}$ is the distance between the RIS and user $\kappa \in \mathcal{K}$ and is constant during the whole flying time.

As shown in Figure 2, we employ the time division multiple access (TDMA) protocol [32]. Specifically, the total flight time, denoted as T, is divided into $S + K$ time slots. The time slots τ_1 to τ_S are designated for DL WPT. The remaining time slots are designated for UL WIT. For ease of notation, τ_{sE} represents the s-th WPT time slot and $\tau_{\kappa I}$ represents the κ-th WIT time slot. The constraint of transmission time allocation

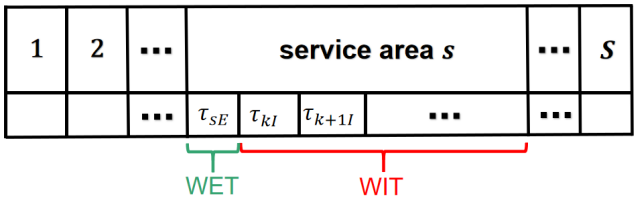

FIGURE 2. The transmission protocol for the RIS-assisted UAV-enabled WPCN.

can be given by

$$\tau_{sE} \geq 0, \forall s \in \mathcal{S}, \tag{1}$$

$$\tau_{\kappa I} \geq 0, \forall \kappa \in \mathcal{K}, \tag{2}$$

$$\sum_{s=1}^{S} \tau_{sE} + \sum_{\kappa=1}^{K} \tau_{\kappa I} = T. \tag{3}$$

In time slot τ_{sE}, the UAV hovers at a fixed place in s service area and transmits power to all the users in that service area at the same time. We define P_1 as the transmit power of UAV in the DL WPT. Due to the payload and power consumption constraints on the UAV, it might be unfeasible to dynamically adjust the transmit power, so we set it as a constant. Despite the fact that the idealistic linear energy harvesting model can only be applied when the energy conversion efficiency is constant throughout an endlessly large range of input power levels, it is shown that the linear energy harvesting model can be reached by concatenating multiple non-linear energy harvesting circuits in parallel [33]. Therefore, the power harvested by the κ-th user in the s-th service area can be expressed as

$$\eta \left| (\boldsymbol{h}_\kappa)^H \boldsymbol{\Theta}_{1,s} \boldsymbol{h}_s + g_{s,\kappa} \right|^2 P_1 \tau_{sE}, \,^{1} \tag{4}$$

where $(\boldsymbol{h}_\kappa)^H \boldsymbol{\Theta}_{1,s} \boldsymbol{h}_s + g_{s,\kappa}$ is the composite channel from UAV to ground users [34], η is the energy conversion efficiency and is required to satisfy $0 < \eta \leq 1$, $\boldsymbol{\Theta}_{1,s} = \text{diag}\left(e^{j\theta_{s,1,1}}, \ldots, e^{j\theta_{s,1,M}}\right)$ is a diagonal reflection coefficient matrix at the RIS in the downlink, where the reflection amplitude is fixed at 1. The variable $\theta_{s,1,i}$ denotes the phase shift of the i-th reflective element. The variables $\boldsymbol{h}_\kappa \in \mathbb{C}^{M\times 1}$, $\boldsymbol{h}_s \in \mathbb{C}^{M\times 1}$ and $g_{s,\kappa}$ denote the channel between the RIS and the ground user $\kappa \in \mathcal{K}$, the channel between the UAV serving as HAP in the $s \in \mathcal{S}$ service area and the RIS, and the channel between the UAV serving as HAP in the $s \in \mathcal{S}$ service area and the ground user $\kappa \in \mathcal{K}$, respectively. Since both the UAV and users are equipped with a single antenna, the downlink and uplink channel can be represented by the same expression.

Then in each time slot $\tau_{\kappa I}$, the user κ sends information signals to the UAV. Because each time slot is separated, there is no interference. We define $P_{2\kappa}$ as the transmit power of user $\kappa \in \mathcal{K}$ using for the UL WIT. Subsequently, the data rate from user $\kappa \in \mathcal{K}$ to the UAV can be expressed as follows.

$$R_\kappa = \frac{\tau_{\kappa I}}{T} \log_2 \left(1 + \frac{P_{2\kappa} \left| (\boldsymbol{h}_\kappa)^H \boldsymbol{\Theta}_{2,\kappa} \boldsymbol{h}_s + g_{s,\kappa} \right|^2}{\sigma^2} \right), \,^{2} \tag{5}$$

where $\boldsymbol{\Theta}_{2,\kappa} = \text{diag}\left(e^{j\theta_{\kappa,2,1}}, \ldots, e^{j\theta_{\kappa,2,M}}\right)$ represents the reflection coefficient matrix at the RIS, and σ^2 is the noise power.

To ensure the self-sustainability of the WPCN, the amount of energy used by the user for the UL WIT cannot go above the amount of energy obtained from the DL WPT. Therefore, the energy constraint is given by

$$\eta \left| (\boldsymbol{h}_\kappa)^H \boldsymbol{\Theta}_{1,s} \boldsymbol{h}_s + g_{s,\kappa} \right|^2 P_1 \tau_{sE} \geq P_{2\kappa} \tau_{\kappa I}, \forall s \in \mathcal{S}, \forall \kappa \in \mathcal{K}. \tag{6}$$

Since the RIS is always placed on top of a building and the UAV flies at high altitude, there is little obstruction or reflection occurring during the transmission between the UAV and the RIS [11]. Therefore, we use a LoS model to represent the channel vector between the UAV and the RIS $\boldsymbol{h}_s$ that can be given by [35]

$$\boldsymbol{h}_s = \sqrt{\frac{\beta_0}{(d_s^{UR})^2}} \left[1, e^{-j2\pi \frac{d\phi_s^{UR}}{\lambda_c}}, \ldots, e^{-j2\pi(M-1)\frac{d\phi_s^{UR}}{\lambda_c}} \right]^T, \tag{7}$$

where β_0 represents the channel power gain at the reference distance $d_0 = 1$ m, $\phi_s^{UR} = \frac{x_R - x_{s,u}}{d_s^{UR}}$, d represents the distance between antennas, λ_c denotes the wavelength of the carrier signal.

On the other hand, in the links from UAV to ground users and from RIS to ground users, we apply the Rician fading channel model taking into account the scattering near ground users [16], [36]. Therefore, the channel $g_{s,\kappa}$ and $\boldsymbol{h}_\kappa$ can be given by

$$g_{s,\kappa} = \sqrt{\frac{\beta_0}{(d_{s,\kappa}^{UG})^{\alpha^{UG}}}} \left(\sqrt{\frac{K_R^{UG}}{1+K_R^{UG}}} + \sqrt{\frac{1}{K_R^{UG}+1}} h_{\kappa,UG}^{NLoS} \right), \tag{8}$$

$$\boldsymbol{h}_\kappa = \sqrt{\frac{\beta_0}{(d_\kappa^{RG})^{\alpha^{RG}}}} \left(\sqrt{\frac{K_R^{RG}}{1+K_R^{RG}}} \boldsymbol{h}_{\kappa,RG}^{LoS} + \sqrt{\frac{1}{K_R^{RG}+1}} \boldsymbol{h}_{\kappa,RG}^{NLoS} \right). \tag{9}$$

where $h_{\kappa,UG}^{NLoS} \sim \mathcal{CN}(0,1)$, $\boldsymbol{h}_{\kappa,RG}^{NLoS} \sim \mathcal{CN}(0,\boldsymbol{I})$ represent the random scattering component, $\boldsymbol{h}_{\kappa,RG}^{LoS} = \left[1, e^{-j2\pi \frac{d\phi_\kappa^{RG}}{\lambda_c}}, \ldots, e^{-j2\pi(M-1)\frac{d\phi_\kappa^{RG}}{\lambda_c}} \right]^T$ denotes the LoS component. α^{UG}, α^{RG} denote the path loss exponent, which can reflect the difference in path loss caused by the gap in propagation distance [36], [37]. K_R^{UG}, K_R^{RG} are the Rician factor controlling the proportion of LoS and NLoS.

[1] We note that our proposed algorithm might not be applicable to the non-linear model, we will leave it for future work.

[2] The data rate obtained through the Shannon formula serves as a theoretical upper limit. Actual performance is expected to be lower than this limit but can approach it infinitely.

In this paper, in order to guarantee the fairness, we maximize the minimum throughput of all the users. Here, the optimization problem can be formulated as follows.

$$\max_{\boldsymbol{w}_{s,u},P_{2\kappa},\tau_{sE},\tau_{\kappa I},\boldsymbol{\Theta}_{1,s},\boldsymbol{\Theta}_{2,\kappa}} \min_{\kappa\in\mathcal{K}} R_\kappa \tag{10a}$$

$$\text{s.t. } \eta\left|(\boldsymbol{h}_\kappa)^H\boldsymbol{\Theta}_{1,s}\boldsymbol{h}_s+g_{s,\kappa}\right|^2 P_1\tau_{sE}\geq P_{2\kappa}\tau_{\kappa I},\forall s\in\mathcal{S},\ \forall\kappa\in\mathcal{K}, \tag{10b}$$

$$P_{2\kappa}\geq 0,\forall\kappa\in\mathcal{K}, \tag{10c}$$

$$(1)-(3). \tag{10d}$$

By introducing an auxiliary variable t, we reformulate the problem (10) as the equivalent problem.

$$\max_{\boldsymbol{w}_{s,u},P_{2\kappa},\tau_{sE},\tau_{\kappa I},\boldsymbol{\Theta}_{1,s},\boldsymbol{\Theta}_{2,\kappa},t} t \tag{11a}$$

$$\text{s.t. } R_\kappa\geq t,\forall\kappa\in\mathcal{K}, \tag{11b}$$

$$(10b)-(10d). \tag{11c}$$

Since the reflection coefficient matrix is highly coupled with the location of the UAV, the minimum throughput maximization problem is non-convex and nonlinear. To tackle this problem, we propose a method that jointly optimizes the horizontal location of UAV, transmit power, transmission time allocation and passive beamforming in sequence.

III. THE ALTERNATING OPTIMIZATION-BASED LOW-COMPLEXITY ALGORITHM

In this part, our algorithm deals with the minimum throughput maximization problem by dividing the primary one into four sub-problems. Since the composite channel gain is contingent upon the placement of the UAV, we obtain the UAV's optimal horizontal location by using SCA to further optimize other variables. Moreover, we determine the optimal transmit power and time allocation with the acquisition of UAV's 2D location. Finally, we optimize the passive beamforming based on the achieved UAV's horizontal location, transmit power and time allocation by applying SDR.

A. OPTIMAL UAV HORIZONTAL LOCATION

Firstly, we optimize $\boldsymbol{w}_{s,u}$ for any given $P_{2\kappa}$, τ_{sE}, $\tau_{\kappa I}$, $\boldsymbol{\Theta}_{1,s}$, $\boldsymbol{\Theta}_{2,\kappa}$, and the problem can be expressed as

$$\max_{\boldsymbol{w}_{s,u},t} t \tag{12a}$$

$$\text{s.t. } \frac{\tau_{\kappa I}}{T}\log_2\left(1+\frac{P_{2\kappa}\left|(\boldsymbol{h}_\kappa)^H\boldsymbol{\Theta}_{2,\kappa}\boldsymbol{h}_s+g_{s,\kappa}\right|^2}{\sigma^2}\right)\geq t,\ \forall s\in\mathcal{S},\forall\kappa\in\mathcal{K}, \tag{12b}$$

$$\eta\left|(\boldsymbol{h}_\kappa)^H\boldsymbol{\Theta}_{1,s}\boldsymbol{h}_s+g_{s,\kappa}\right|^2 P_1\tau_{sE}\geq P_{2\kappa}\tau_{\kappa I},\forall s\in\mathcal{S},\forall\kappa\in\mathcal{K}. \tag{12c}$$

To facilitate the solution, the channel $\boldsymbol{h}_\kappa$ can be expressed as $\boldsymbol{h}_\kappa = \left[\left|h_{\kappa,1}\right|e^{j\varphi_1},\ldots,\left|h_{\kappa,M}\right|e^{j\varphi_M}\right]^T$, where $\left|h_{\kappa,i}\right|$ is the amplitude of the i-th element of $\boldsymbol{h}_\kappa$ and $\varphi_i\in[0,2\pi)$ is its phase shift. By introducing the new expression of $\boldsymbol{h}_\kappa$, the composite channel is given by

$$(\boldsymbol{h}_\kappa)^H\boldsymbol{\Theta}_{2,\kappa}\boldsymbol{h}_s=\frac{\sqrt{\beta_0}\sum_{i=1}^M\left|h_{\kappa,i}\right|e^{j\left(\theta_{2,i}-\varphi_i-2\pi\frac{d(i-1)}{\lambda_c}\phi_s^{UR}\right)}}{d_s^{UR}}. \tag{13}$$

Similarly, $g_{s,\kappa}$ can be expressed as below

$$\begin{aligned}g_{s,\kappa}&=\sqrt{\frac{\beta_0}{(d_{s,\kappa}^{UG})^{\alpha^{UG}}}}\left(\sqrt{\frac{K_R^{UG}}{1+K_R^{UG}}}+\sqrt{\frac{1}{K_R^{UG}+1}}h_{\kappa,UG}^{NLoS}\right)\\&=\frac{\left|G_{s,k}\right|}{(d_{s,\kappa}^{UG})^{\frac{\alpha^{UG}}{2}}}e^{j\zeta}.\end{aligned} \tag{14}$$

Using the equations (13) and (14), the composite channel power gain between the UAV and users is given by

$$\begin{aligned}&\left|(\boldsymbol{h}_\kappa)^H\boldsymbol{\Theta}_{2,\kappa}\boldsymbol{h}_s+g_{s,\kappa}\right|^2\\&=\left(\frac{\left|G_{s,\kappa}\right|}{(d_{s,\kappa}^{UG})^{\frac{\alpha^{UG}}{2}}}\right)^2+\left(\frac{\sqrt{\beta_0}\sum_{i=1}^M\left|h_{\kappa,i}\right|}{d_s^{UR}}\right)^2\\&\quad+2\frac{\sqrt{\beta_0}\left|G_{s,k}\right|\sum_{i=1}^M\left|h_{\kappa,i}\right|}{d_s^{UR}(d_{s,\kappa}^{UG})^{\frac{\alpha^{UG}}{2}}}\\&\quad\times cos\left(\theta_{2,i}-\varphi_i-2\pi\frac{d\,(i-1)}{\lambda_c}\phi_s^{UR}-\zeta\right).\end{aligned} \tag{15}$$

The minimum boundary of the composite channel power gain is used to tighten the constraints. Therefore, considering properties of the cosine function and $\sqrt{\beta_0}\left|G_{s,k}\right|\sum_{i=1}^M\left|h_{\kappa,i}\right|>0$, the composite channel power gain will be minimized in the following condition.

$$\theta_{2,i}-\varphi_i-2\pi\frac{d\,(i-1)}{\lambda_c}\phi_s^{UR}=\zeta+\pi+2m\pi,m=0,1,2,\ldots, \tag{16}$$

The minimum boundary of the composite channel power gain is given by

$$\begin{aligned}\left|(\boldsymbol{h}_\kappa)^H\boldsymbol{\Theta}_{2,\kappa}\boldsymbol{h}_s+h_{s,\kappa}\right|^2\geq&\left(\frac{\left|G_{s,k}\right|}{(d_{s,\kappa}^{UG})^{\frac{\alpha^{UG}}{2}}}\right)^2+\left(\frac{\sqrt{\beta_0}\sum_{i=1}^M\left|h_{\kappa,i}\right|}{d_s^{UR}}\right)^2\\&-2\frac{\sqrt{\beta_0}\left|G_{s,k}\right|\sum_{i=1}^M\left|h_{\kappa,i}\right|}{d_s^{UR}(d_{s,\kappa}^{UG})^{\frac{\alpha^{UG}}{2}}},\\&\forall s\in\mathcal{S},\forall\kappa\in\mathcal{K}.\end{aligned} \tag{17}$$

By adopting the lower bound of the throughput in (12b) and the minimum composite channel power gain mentioned above, we transform (12b) into the following expression

$$\left(\frac{|G_{s,k}|}{(d_{s,\kappa}^{UG})^{\frac{\alpha^{UG}}{2}}}\right)^2+\left(\frac{\sqrt{\beta_0}\sum_{i=1}^{M}|h_{\kappa,i}|}{d_s^{UR}}\right)^2\geq\frac{\sigma^2}{P_{2\kappa}}\left(2^{\frac{tT}{\tau_{\kappa I}}}-1\right)+2\frac{\sqrt{\beta_0}|G_{s,k}|\sum_{i=1}^{M}|h_{\kappa,i}|}{d_s^{UR}(d_{s,\kappa}^{UG})^{\frac{\alpha^{UG}}{2}}},\forall s\in\mathcal{S},\ \forall\kappa\in\mathcal{K}. \tag{18}$$

However, (18) remains non-convex with respect to $\boldsymbol{w}_{s,u}$ due to the nonlinearity of $d_{s,\kappa}^{UG}$ and d_s^{UR}. Therefore, $p_{s,\kappa}$ and q_s are employed as slack variables to solve the non-convexity of (18) where $d_{s,\kappa}^{UG}\leq p_{s,\kappa}$ and $d_s^{UR}\leq q_s$. In this case, (18) can be reformulated as

$$\frac{|G_{s,k}|^2}{p_{s,\kappa}^{\alpha^{UG}}}+\frac{\left(\sqrt{\beta_0}\sum_{i=1}^{M}|h_{\kappa,i}|\right)^2}{q_s^2}\geq\frac{\sigma^2}{P_{2\kappa}}\left(2^{\frac{tT}{\tau_{\kappa I}}}-1\right)+2\frac{\sqrt{\beta_0}|G_{s,k}|\sum_{i=1}^{M}|h_{\kappa,i}|}{q_sp_{s,\kappa}^{\frac{\alpha^{UG}}{2}}},\forall s\in\mathcal{S},\forall\kappa\in\mathcal{K}, \tag{19}$$

we denote $X_\kappa=|G_{s,k}|^2$, $Y_\kappa=\left(\sqrt{\beta_0}\sum_{i=1}^{M}|h_{\kappa,i}|\right)^2$, $Z_\kappa=2\sqrt{\beta_0}|G_{s,k}|\sum_{i=1}^{M}|h_{\kappa,i}|$.

We restructure (19) into a convex optimization problem by using the disciplined convex programming (DCP) [38]. It is evident that the expression $\frac{\sigma^2}{P_{2\kappa}}\left(2^{\frac{tT}{\tau_{\kappa I}}}-1\right)$ is convex with respect to the variable t. Moreover, $\frac{|G_{s,k}|^2}{p_{s,\kappa}^{\alpha^{UG}}}+\frac{\left(\sqrt{\beta_0}\sum_{i=1}^{M}|h_{\kappa,i}|\right)^2}{q_s^2}$ and $2\frac{\sqrt{\beta_0}|G_{s,k}|\sum_{i=1}^{M}|h_{\kappa,i}|}{q_sp_{s,\kappa}^{\frac{\alpha^{UG}}{2}}}$ are convex according to Lemma 1.

Lemma 1: Given $K_1>0, K_2>0, K_3>0$, $F(m,n)=\frac{K_1}{m^\kappa}+\frac{K_2}{n^2}$ and $G(m,n)=\frac{K_3}{m^{\frac{\kappa}{2}}n}$ are convex with respect to $m>0, n>0$.

Proof: See the Appendix A. ■

It should be noted that the first-order Taylor approximation of the convex function is a global under-estimator. We define slack variables as $p_{s,\kappa}^{(l)}$ and $q_s^{(l)}$, where $l\geq0$ is the iteration number. $p_{s,\kappa}^{(0)}$ and $q_s^{(0)}$ denote the initial variables. Hence, the first-order Taylor approximation of $\frac{X_\kappa}{p_{s,\kappa}^{\alpha^{UG}}}+\frac{Y_\kappa}{q_s^2}$, $p_{s,\kappa}^2$, q_s^2 at the given points $p_{s,\kappa}^{(l-1)}$ and $q_s^{(l-1)}$ can be expressed as (20), shown at the bottom of the next page, and (21) - (22):

$$p_{s,\kappa}^2\geq\left(p_{s,\kappa}^{(l-1)}\right)^2+2p_{s,k}^{(l-1)}\left(p_{s,\kappa}-p_{s,\kappa}^{(l-1)}\right),\forall s\in\mathcal{S},\forall\kappa\in\mathcal{K}, \tag{21}$$

$$q_s^2\geq\left(q_s^{(l-1)}\right)^2+2q_s^{(l-1)}\left(q_s-q_s^{(l-1)}\right),\forall s\in\mathcal{S}. \tag{22}$$

Therefore, (19) can be reformulated as (23), shown at the bottom of the next page, by applying (20) and the energy constraint (12c) can be reformulated as (24), shown at the bottom of the next page.

Consequently, the UAV 2D location optimization problem (12) can be represented as

$$\max_{\boldsymbol{w}_{s,u},p_{s,\kappa},q_s,t}\ t \tag{25a}$$

$$\text{s.t. (23)}-\text{(24)}, \tag{25b}$$

$$d_{s,\kappa}^{UG2}-2p_{s,\kappa}^{(l-1)}p_{s,\kappa}+\left(p_{s,\kappa}^{(l-1)}\right)^2\leq0,\forall s\in\mathcal{S},\forall\kappa\in\mathcal{K}, \tag{25c}$$

$$d_s^{UR2}-2q_s^{(l-1)}q_s+\left(q_s^{(l-1)}\right)^2\leq0,\forall s\in\mathcal{S}. \tag{25d}$$

Since problem (25) is a convex optimization problem, an optimization toolbox like the MOSEK can be used to solve it [39].

B. OPTIMAL TRANSMIT POWER

In this part, the transmit power optimization problem can be provided by

$$\max_{P_{2\kappa},t}\ t$$

$$\text{s.t. }\frac{\tau_{\kappa I}}{T}\log_2\left(1+\frac{P_{2\kappa}\left|(\boldsymbol{h}_\kappa)^H\boldsymbol{\Theta}_{2,\kappa}\boldsymbol{h}_s+g_{s,\kappa}\right|^2}{\sigma^2}\right)\geq t,\forall s\in\mathcal{S},\forall\kappa\in\mathcal{K}, \tag{26a}$$

$$\frac{\eta\left|(\boldsymbol{h}_\kappa)^H\boldsymbol{\Theta}_{1,s}\boldsymbol{h}_s+g_{s,\kappa}\right|^2P_1\tau_{sE}}{\tau_{\kappa I}}\geq P_{2\kappa}\geq0,\forall s\in\mathcal{S},\forall\kappa\in\mathcal{K}. \tag{26b}$$

Since energy conversion efficiency η, transmission time allocation τ_{sE} and $\tau_{\kappa I}$, transmit power of the UAV P_1 are all non-negative, we obtain the composite channel which holds $\frac{\eta|(\boldsymbol{h}_\kappa)^H\boldsymbol{\Theta}_{1,s}\boldsymbol{h}_s+g_{s,\kappa}|^2P_1\tau_{sE}}{\tau_{\kappa I}}\geq0,\forall s\in\mathcal{S},\forall\kappa\in\mathcal{K}$. Note that $\frac{\tau_{\kappa I}}{T}\log_2\left(1+\frac{P_{2\kappa}|(\boldsymbol{h}_\kappa)^H\boldsymbol{\Theta}_{2,\kappa}\boldsymbol{h}_s+g_{s,\kappa}|^2}{\sigma^2}\right)$ is monotonic increasing with respect to $P_{2\kappa}$ when $\frac{\tau_{\kappa I}}{T}\geq0$ and $\frac{|(\boldsymbol{h}_\kappa)^H\boldsymbol{\Theta}_{2,\kappa}\boldsymbol{h}_s+g_{s,\kappa}|^2}{\sigma^2}\geq0$. Thus, the optimal solution of problem (26) can be given by

$$P_{2\kappa}^*=\frac{\eta\left|(\boldsymbol{h}_\kappa)^H\boldsymbol{\Theta}_{1,s}\boldsymbol{h}_s+g_{s,\kappa}\right|^2P_1\tau_{sE}}{\tau_{\kappa I}},\forall s\in\mathcal{S},\forall\kappa\in\mathcal{K}, \tag{27}$$

$$t^*=\min_{\kappa\in\mathcal{K}}\left\{\frac{\tau_{\kappa I}}{T}\log_2\left(1+\frac{P_{2\kappa}^*\left|(\boldsymbol{h}_\kappa)^H\boldsymbol{\Theta}_{2,\kappa}\boldsymbol{h}_s+g_{s,\kappa}\right|^2}{\sigma^2}\right)\right\},\ \forall s\in\mathcal{S},\forall\kappa\in\mathcal{K}. \tag{28}$$

C. OPTIMAL TRANSMISSION TIME ALLOCATION

Based on the obtained 2D location of the UAV $\boldsymbol{w}_{s,u}$ and optimal transmit power $P_{2\kappa}$, we fix the passive beamforming

vector $\boldsymbol{\Theta}_{1,s}$, $\boldsymbol{\Theta}_{2,\kappa}$ and rewrite the problem as

$$\max_{\tau_{sE},\tau_{\kappa I},t} \quad t \tag{29a}$$

$$\text{s.t.} \ \frac{\tau_{\kappa I}}{T}\log_2\left(1+\frac{P_{2\kappa}\left|(\boldsymbol{h}_\kappa)^H\boldsymbol{\Theta}_{2,\kappa}\boldsymbol{h}_s+g_{s,\kappa}\right|^2}{\sigma^2}\right)\geq t,$$
$$\forall s\in\mathcal{S},\forall\kappa\in\mathcal{K}, \tag{29b}$$

$$\eta P_1\tau_{sE}\left|(\boldsymbol{h}_\kappa)^H\boldsymbol{\Theta}_{1,s}\boldsymbol{h}_s+g_{s,\kappa}\right|^2\geq P_{2\kappa}\tau_{\kappa I},\forall s\in\mathcal{S},\forall\kappa\in\mathcal{K}, \tag{29c}$$

$$(1)-(3). \tag{29d}$$

Since problem (29) is a linear programming problem, solvers like the CVX can be used to solve it [40].

D. OPTIMAL PASSIVE BEAMFORMING VECTOR

With the variables that have been resolved above, we finally optimize the passive beamforming $\boldsymbol{\Theta}_{1,s}$ and $\boldsymbol{\Theta}_{2,\kappa}$. The problem of optimizing passive beamforming can be simplified as

$$\max_{\boldsymbol{\Theta}_{1,s},\boldsymbol{\Theta}_{2,\kappa},t} \quad t \tag{30a}$$

$$\text{s.t.} \ \left|(\boldsymbol{h}_\kappa)^H\boldsymbol{\Theta}_{2,\kappa}\boldsymbol{h}_s+g_{s,\kappa}\right|^2\geq\frac{\sigma^2}{P_{2\kappa}}\left(2^{\frac{tT}{\tau_{\kappa I}}}-1\right),\forall s\in\mathcal{S},$$
$$\forall\kappa\in\mathcal{K}, \tag{30b}$$

$$\eta\left|(\boldsymbol{h}_\kappa)^H\boldsymbol{\Theta}_{1,s}\boldsymbol{h}_s+g_{s,\kappa}\right|^2P_1\tau_{sE}\geq P_{2\kappa}\tau_{\kappa I},\forall s\in\mathcal{S},\forall\kappa\in\mathcal{K}. \tag{30c}$$

Letting $\boldsymbol{v}_{1,s}=\left[e^{j\theta_{s,1,1}},\ldots,e^{j\theta_{s,1,M}}\right]^H$ denote the passive beamforming in the DL, we can reformulate the composite channel gain from UAV to user $\kappa\in\mathcal{K}$ as $(\boldsymbol{h}_\kappa)^H\boldsymbol{\Theta}_{1,s}\boldsymbol{h}_s=\boldsymbol{v}_{1,s}^H\boldsymbol{\Phi}_\kappa$, where $\boldsymbol{\Phi}_\kappa=\text{diag}\left(\boldsymbol{h}_\kappa{}^H\right)\boldsymbol{h}_s$. As for the reflective channel, we introduce the notations $\boldsymbol{v}_{2,\kappa}=\left[e^{j\theta_{\kappa,2,1}},\ldots,e^{j\theta_{\kappa,2,M}}\right]^H$, $(\boldsymbol{h}_\kappa)^H\boldsymbol{\Theta}_{2,\kappa}\boldsymbol{h}_s=\boldsymbol{v}_{2,\kappa}^H\boldsymbol{\Phi}_\kappa$. Consequently, we have

$$\left|(\boldsymbol{h}_\kappa)^H\boldsymbol{\Theta}_j\boldsymbol{h}_s+g_{s,\kappa}\right|^2=\boldsymbol{v}_j^HQ_\kappa\boldsymbol{v}_j+2Re\left\{\boldsymbol{v}_j^HD_\kappa\right\}+\left|g_{s,\kappa}\right|^2,$$
$$j=(1,s),(2,\kappa), \tag{31}$$

where $Q_\kappa=\boldsymbol{\Phi}_\kappa\boldsymbol{\Phi}_\kappa^H$, $D_\kappa=\boldsymbol{\Phi}_\kappa g_{s,\kappa}^H$. Then the equivalent problem is given by

$$\max_{\boldsymbol{v}_{1,s},\boldsymbol{v}_{2,\kappa},t} \quad t \tag{32a}$$

$$\text{s.t.} \ \left|v_j\right|=1,j=(1,s),(2,\kappa). \tag{32b}$$

$$\boldsymbol{v}_{2,\kappa}^HQ_\kappa\boldsymbol{v}_{2,\kappa}+2Re\left\{\boldsymbol{v}_{2,\kappa}^HD_\kappa\right\}+\left|g_{s,\kappa}\right|^2\geq\frac{\sigma^2}{P_{2\kappa}}\left(2^{\frac{tT}{\tau_{\kappa I}}}-1\right),$$
$$\forall s\in\mathcal{S},\forall\kappa\in\mathcal{K}, \tag{32c}$$

$$\eta P_1\tau_{sE}\left(\boldsymbol{v}_{1,s}^HQ_\kappa\boldsymbol{v}_{1,s}+2Re\left\{\boldsymbol{v}_{1,s}^HD_\kappa\right\}+\left|g_{s,\kappa}\right|^2\right)\geq P_{2\kappa}\tau_{\kappa I},$$
$$\forall s\in\mathcal{S},\forall\kappa\in\mathcal{K}, \tag{32d}$$

Problem (32) is still non-convex. Inspired by [41], we apply SDR to solve problem (32). We first define $\left|(\boldsymbol{h}_\kappa)^H\boldsymbol{\Theta}_j\boldsymbol{h}_s+g_{s,\kappa}\right|^2=\bar{\boldsymbol{v}}_j^HR_\kappa\bar{\boldsymbol{v}}_j+\left|g_{s,\kappa}\right|^2,j=(1,s),(2,\kappa)$, where

$$R_\kappa=\begin{bmatrix}Q_\kappa & D_\kappa\\ D_\kappa^H & 0\end{bmatrix},\bar{\boldsymbol{v}}_j=\begin{bmatrix}\boldsymbol{v}_j\\ 1\end{bmatrix}. \tag{33}$$

$$\frac{X_\kappa}{p_{s,\kappa}^{\alpha^{UG}}}+\frac{Y_\kappa}{q_s^2}\geq\left(\frac{X_\kappa}{\left(p_{s,\kappa}^{(l-1)}\right)^{\alpha^{UG}}}+\frac{Y_\kappa}{\left(q_s^{(l-1)}\right)^2}\right)-\frac{\alpha^{UG}X_\kappa}{\left(p_{s,\kappa}^{(l-1)}\right)^{\alpha^{UG}+1}}\left(p_{s,\kappa}-p_{s,\kappa}^{(l-1)}\right)-\frac{2Y_\kappa}{\left(q_s^{(l-1)}\right)^3}\left(q_s-q_s^{(l-1)}\right),$$
$$\forall s\in\mathcal{S},\forall\kappa\in\mathcal{K}, \tag{20}$$

$$\left(\frac{X_\kappa}{\left(p_{s,\kappa}^{(l-1)}\right)^{\alpha^{UG}}}+\frac{Y_\kappa}{\left(q_s^{(l-1)}\right)^2}\right)-\frac{\alpha^{UG}X_\kappa}{\left(p_{s,\kappa}^{(l-1)}\right)^{\alpha^{UG}+1}}\left(p_{s,\kappa}-p_{s,\kappa}^{(l-1)}\right)-\frac{2Y_\kappa}{\left(q_s^{(l-1)}\right)^3}\left(q_s-q_s^{(l-1)}\right)$$
$$\geq\frac{\sigma^2}{P_{2\kappa}}\left(2^{\frac{tT}{\tau_{\kappa I}}}-1\right)+\frac{Z_\kappa}{q_sp_{s,\kappa}^{\frac{\alpha^{UG}}{2}}},\forall s\in\mathcal{S},\forall\kappa\in\mathcal{K}. \tag{23}$$

$$\eta P_1\tau_{sE}\left(\left(\frac{X_\kappa}{\left(p_{s,\kappa}^{(l-1)}\right)^{\alpha^{UG}}}+\frac{Y_\kappa}{\left(q_s^{(l-1)}\right)^2}\right)-\frac{\alpha^{UG}X_\kappa}{\left(p_{s,\kappa}^{(l-1)}\right)^{\alpha^{UG}+1}}\left(p_{s,\kappa}-p_{s,\kappa}^{(l-1)}\right)-\frac{2Y_\kappa}{\left(q_s^{(l-1)}\right)^3}\left(q_s-q_s^{(l-1)}\right)\right)$$
$$\geq\eta P_1\tau_{sE}\frac{Z_\kappa}{q_sp_{s,\kappa}^{\frac{\alpha^{UG}}{2}}}+P_{2\kappa}\tau_{\kappa I},\forall s\in\mathcal{S},\forall\kappa\in\mathcal{K}. \tag{24}$$

Consequently, problem (32) can be transformed as

$$\max_{\bar{\boldsymbol{v}_{1,s}},\bar{\boldsymbol{v}_{2,\kappa}},t} \quad t \tag{34a}$$

$$\text{s.t. } \left|\bar{v}_j\right| = 1, j = (1,s),(2,\kappa), \tag{34b}$$

$$\bar{\boldsymbol{v}_{2,\kappa}}^H \boldsymbol{R}_\kappa \bar{\boldsymbol{v}_{2,\kappa}} + \left|g_{s,\kappa}\right|^2 \geq \frac{\sigma^2}{P_{2\kappa}} \left(2^{\frac{tT}{\tau_{\kappa I}}} - 1\right), \forall s \in \mathcal{S}, \forall \kappa \in \mathcal{K}, \tag{34c}$$

$$\eta P_1 \tau_{sE} \left(\bar{\boldsymbol{v}_{1,s}}^H \boldsymbol{R}_\kappa \bar{\boldsymbol{v}_{1,s}} + \left|g_{s,\kappa}\right|^2\right) \geq P_{2\kappa} \tau_{\kappa I}, \forall s \in \mathcal{S}, \forall \kappa \in \mathcal{K}, \tag{34d}$$

Note that the constraints of problem (34) are linear with the matrix $\bar{\boldsymbol{v}_j}\bar{\boldsymbol{v}_j}^H, j = (1,s),(2,\kappa)$. Thus, we define $\boldsymbol{V}_j = \bar{\boldsymbol{v}_j}\bar{\boldsymbol{v}_j}^H, j = (1,s),(2,\kappa)$ with $\boldsymbol{V}_j \succeq 0$ and $\text{rank}(\boldsymbol{V}_j) = 1$. We use the SDR approach to relax the rank-one restriction [41]. Therefore, the problem is expressed as

$$\max_{\boldsymbol{V}_{1,s},\boldsymbol{V}_{2,\kappa},t} \quad t \tag{35a}$$

$$\text{s.t. } \boldsymbol{V}_j \succeq 0, j = (1,s),(2,\kappa), \tag{35b}$$

$$\left[V_j\right]_{m,m} = 1, m = 1,\ldots,M+1, \quad j = (1,s),(2,\kappa), \tag{35c}$$

$$Tr\left(\boldsymbol{R}_\kappa \boldsymbol{V}_{2,\kappa}\right) + \left|g_{s,\kappa}\right|^2 \geq \frac{\sigma^2}{P_{2\kappa}} \left(2^{\frac{tT}{\tau_{\kappa I}}} - 1\right), \forall s \in \mathcal{S}, \forall \kappa \in \mathcal{K}, \tag{35d}$$

$$\eta P_1 \tau_{sE} \left(Tr\left(\boldsymbol{R}_\kappa \boldsymbol{V}_{1,s}\right) + \left|g_{s,\kappa}\right|^2\right) \geq P_{2\kappa} \tau_{\kappa I}, \forall s \in \mathcal{S}, \forall \kappa \in \mathcal{K}, \tag{35e}$$

It is apparent that problem (35) is a convex SDP and can be easily resolved by CVX [40].

However, problem (35) may not guarantee a rank-one solution. Therefore, the Gaussian randomization procedure should be employed when $\text{rank}(\boldsymbol{V}_j^*) > 1$. Firstly, we apply the eigenvalue decomposition to $\boldsymbol{V}_j^*$, where $\boldsymbol{V}_j^* = \boldsymbol{P}_j \boldsymbol{\Lambda}_j \boldsymbol{P}_j^H$. Then we set $\tilde{\boldsymbol{v}_j} = \boldsymbol{P}_j \boldsymbol{\Lambda}_j \boldsymbol{r}_j$, where $\boldsymbol{r} \sim \mathcal{CN}(0, \boldsymbol{I})$. Therefore, the feasible solution to problem (34) can be denoted as $\bar{\boldsymbol{v}_j}$, and $[\bar{\boldsymbol{v}_j}]_n = e^{j \arg([\tilde{\boldsymbol{v}_j}]_n / [\tilde{\boldsymbol{v}_j}]_{M+1})}, n = 1,\ldots,M+1$. A significant number of randomization processes must be used to ensure accuracy. We define $\bar{\boldsymbol{v}_j^*}$ as the best solution and the final solution of problem (35) is $\bar{\boldsymbol{v}_j^*}\bar{\boldsymbol{v}_j^*}^H$. Therefore, based on (33), we obtain the optimal passive beamforming of the RIS.

The following Algorithm 1 summarizes the overall algorithm.

Algorithm 1 Alternating Optimization-Based Low-Complexity Algorithm

Input: $p_{s,\kappa}^{(0)}, q_s^{(0)}, P_{2\kappa}^{(0)}, \tau_{sE}^{(0)}$ and $\tau_{\kappa I}^{(0)}$;
Output: $\boldsymbol{w}_{s,u}^*, P_{2\kappa}^*, \tau_{sE}^*, \tau_{\kappa I}^*, \boldsymbol{\Theta}_{1,s}^*$ and $\boldsymbol{\Theta}_{2,\kappa}^*$;

```
while the increase of the objective function in (10a) is smaller than ε2 do
    while the increase of the objective function in (10a) is smaller than ε1 do
        Update UAV's horizontal hovering location w_{s,u} by solving problem (25), transmit power P_{2κ} based on (27) and transmission time allocation τ_{sE} and τ_{κI} by solving problem (29)
    end while
    Update passive beamforming Θ_{1,s} and Θ_{2,κ} by solving SDP in (35)
end while
```

IV. NUMERICAL RESULTS

In this part of the paper, we offer numerical findings to assess the effectiveness of our suggested method for solving the problem of minimum throughput maximization. The simulation fixes the altitude of UAV at $h = 60$ m and the RIS is positioned at (0, 0, 40 m) [42]. The transmit power of UAV is set as $P_1 = 30$ dBm. The total duration of flight T is equal to 1s. The quantity of reflective elements M is equal to 8. The path-loss exponents α^{UG} and α^{RG} are equal to 2.5. The Rician factor K_R^{UG} and K_R^{RG} is 0 and 8, respectively [16]. Other parameters are set as follows: $d = \frac{\lambda_c}{2}, \sigma^2 = -90$ dBm, $\beta_0 = -20$ dB, $\eta = 0.5$. Considering $h_{\kappa,UG}^{NLoS}$ and $\boldsymbol{h}_{\kappa,RG}^{NLoS}$ are contained in the objective function (10a), we apply their statistical average values to obtain the following numerical results.

To show the performance of the proposed WPCN, we compare with the following benchmark algorithms:

- **Optimal Hovering Location with RIS and UAV:** To compare the performance of dynamic RIS and static RIS, we study "Optimal Hovering Location with Dynamic RIS and UAV" scheme (referred to as DRIS-UAV-OH) and "Optimal Hovering Location with Static RIS and UAV" scheme (referred to as SRIS-UAV-OH). For "Optimal Hovering Location with Dynamic RIS and UAV" scheme, the passive beamforming in UL and DL is different; For "Optimal Hovering Location with Static RIS and UAV" scheme, we optimize the hovering location of UAV with the same phase-shift in DL and UL transmissions.
- **Fixed HAP with RIS and without UAV:** In this scheme, we investigate resource allocation in the RIS-assisted WPCN as proposed in [27] to show the contribution of the UAV. The HAP is deployed at (0, 0, 60 m) and the minimum throughput is maximized by alternatively optimizing the transmit power, transmission time allocation and passive beamforming. To consider the effect of dynamic RIS and static RIS, we study "Fixed HAP with Dynamic RIS and without UAV" scheme (referred to as DRIS-NUAV) and "Fixed HAP with Static RIS and Without UAV" scheme (referred to as SRIS-NUAV).
- **Optimal Hovering Location with UAV and without RIS:** In this scheme, we study the proposed algorithm for UAV-enabled WPCN in [21] to present the benefit brought by the RIS (referred to as NRIS-UAV-OH). The optimization objective and variables are the same

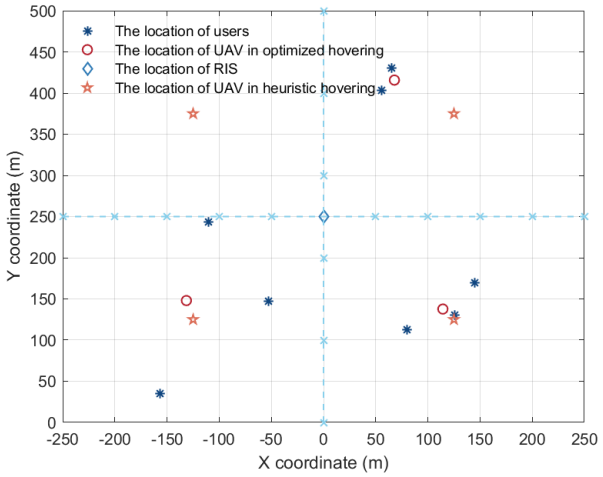

FIGURE 3. The spatial positioning of members within the system.

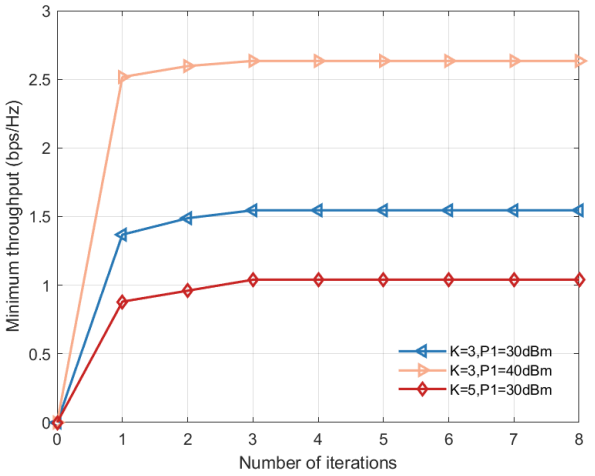

FIGURE 4. The convergence behavior exhibited by the proposed algorithm.

as the mentioned problems except for the RIS passive beamforming.

- **Heuristic Hovering Location with RIS and UAV:** In this scheme, we study the heuristic hovering location algorithm for RIS-assisted UAV-enabled WPCN. In particular, the hovering location of UAV is fixed to the center of each service area. Based on the hovering location of UAV, other variables are optimized according to the algorithm as proposed [42]. To further investigate the benefit brought by RIS, we study the "Heuristic Hovering with Dynamic RIS" (referred to as DRIS-UAV-HH) and the "Heuristic Hovering without RIS" (referred to as NRIS-UAV-HH).

We first visualize the 2D hovering location of UAV determined by our low-complexity algorithm. We assume that $K = 8$ ground users are arranged at random in a 500 m $\times$ 500 m square area, and divide the whole square area into $S = 4$ service areas, where the size of each service area is the same. The RIS is set up in the middle at a height of 40 m. As shown in Figure 3, although there are $S = 4$ service areas, the UAV will skip the area without users because the UAV will follow the optimal hovering location to maximize the throughput of users, and consequently avoid wasting energy to travel every service area. However, in the heuristic hovering algorithm, the UAV will hover at the service area without user which decreases the throughput of the system. Besides, due to the high flexibility, the UAV can stop at any place to deliver wireless communications, which solves the near-far fairness problem for the users positioned on the cell's edge. Therefore, it is found in Figure 3 that the distance from optimized hovering place of UAV to most users in one service area nearly keeps equal to ensure that all users are treated fairly while the heuristic hovering location might be far from the cluster of users.

To demonstrate the convergence properties of our algorithm, we examine three distinct situations: 1) $K = 3$ and $P_1 = 30$ dBm; 2) $K = 3$ and $P_1 = 40$ dBm; 3) $K = 5$ and $P_1 = 30$ dBm; The number of service areas is set as

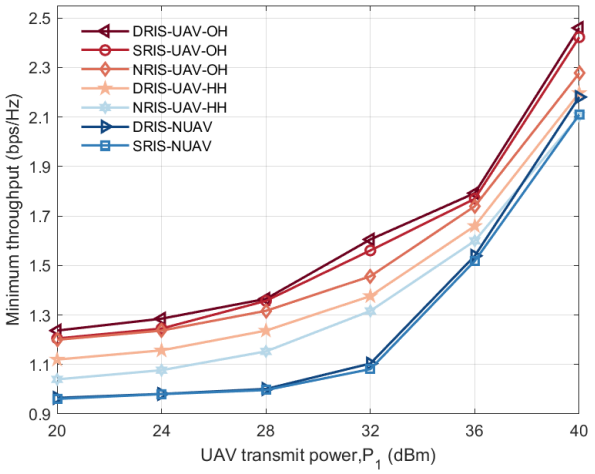

FIGURE 5. The relationship between the minimum throughput and the transmission power of the UAV.

$S = 1$ and the other parameters are configured as described above. It is observed in Figure 4 that for these three cases, the value of the minimum throughput increases monotonically when the quantity of iterations augments, and converges to a certain value. The effectiveness of the algorithm is illustrated by the convergence performance of the minimum throughput. A further indication of rapid convergence of the low-complexity algorithm is that the minimum throughput in all circumstances converges within three iterations. This is because SCA is an efficient algorithm, which accelerates the convergence rate by approximation approaches, and the inner layer of the algorithm speeds up finding the suboptimal solution of the outer layer.

We then investigate the impact of transmit power of the UAV to the minimum throughput performance. We set $K = 3$, $S = 1$ and the rest of parameters are set as above. As the transmit power of the UAV grows, the minimum throughput obtained by all schemes rises, as illustrated in Figure 5. This is explained by the fact that the charging time

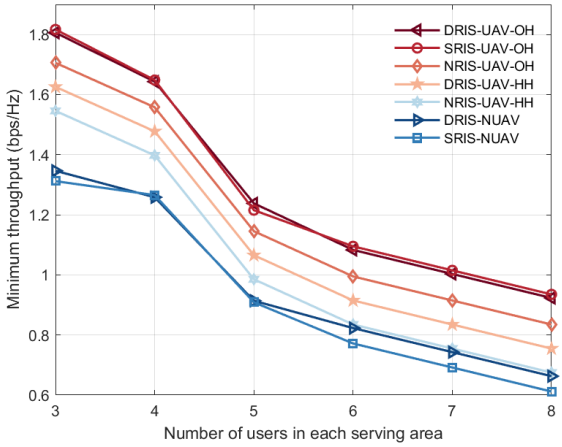

FIGURE 6. The relationship between the minimum throughput and the number of users within each designated service area.

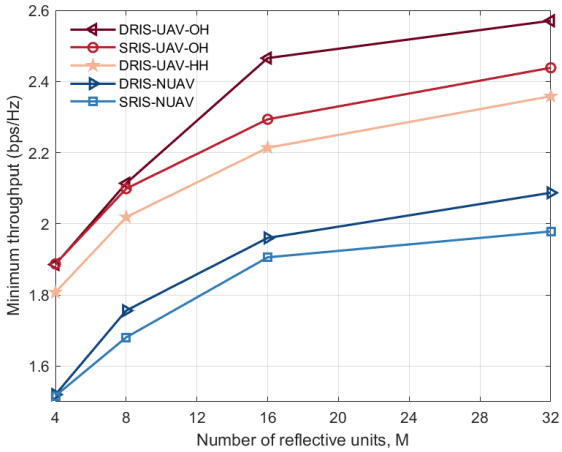

FIGURE 7. The relationship between the minimum throughput and the number of reflective elements in a RIS.

of the UAV will be shortened when the transmit power of UAV increases. Therefore, more time will be allocated to WIT, resulting in the larger minimum throughput. Besides, the minimum throughput of "DRIS-UAV-OH" scheme and "SRIS-UAV-OH" scheme outperform the other cases, which demonstrates that the UAV can establish LoS communication links by adjusting the position of UAV and the RIS can achieve the similar performance of MIMO by designing reflective coefficients. However, in "DRIS-UAV-HH" and "NRIS-UAV-HH", there might be fairness problem that decreases the minimum throughput. Additionally, since the transmit power of the UAV is large enough to shorten the DL WPT time, the performance gap between "DRIS-UAV-OH" and "SRIS-UAV-OH" can be negligible. This reveals that we could adopt a static RIS to decrease the computational complexity of the algorithm.

Figure 6 depicts the minimum throughput versus the number of users in each service area, where we set $P_1 = 35$ dBm, $M = 8$ and other parameters as mentioned above. It is shown that when the number of ground users in one service area increases, the minimum throughput becomes lower. This is as a result of the TDMA protocol's tendency

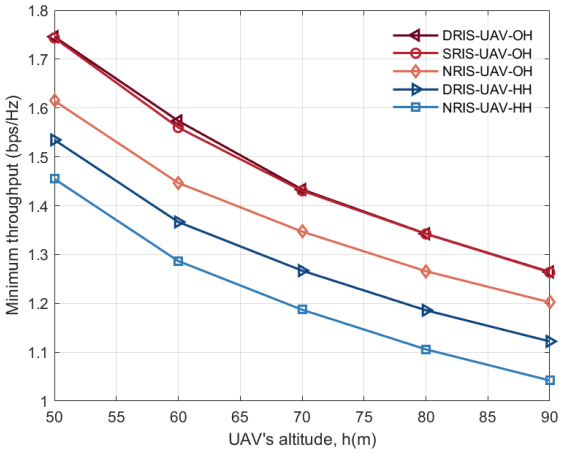

FIGURE 8. The relationship between the minimum throughput and the altitude of the UAV.

to reduce the available WIT as user's number rises, which lowers minimum throughput. In addition, when the number of users increases, the probability of users located at the cell edge will increase, leading to the fairness problem and decrease of minimum throughput. Therefore, when the number of users increases, more hovering points could be set to prevent the fairness problem instead of using the heuristic hovering scheme.

Next, we graph the minimum throughput against the number of reflective units in the RIS as shown in Figure 7, where the transmit power of UAV is set as $P_1 = 35$ dBm and other parameters remain unchanged. The passive beamforming gain would grow with more reflecting units, which would be advantageous to both the DL WET and the UL WIT. As a result, the minimum throughput in all of the schemes increases monotonically as the number of reflective units M rises. Furthermore, our results demonstrate the gap in performance between dynamic RIS and static RIS in the same background becomes more pronounced as the number of reflective units increases. This is expected since a dynamic RIS is required to optimize additional degrees of phase shift for the UL WIT.

Finally, we study the throughput performance under different altitudes of UAV. We assume that there is a single service area with $K = 3$ and $P_1 = 35$ dBm. It is well-known that when the distance increases, the distance-based path loss will be exacerbated. As shown in Figure 8, when the altitude of UAV increases, the minimum throughput decreases. However, if the height of UAV is set too low, its coverage area will not be large enough to serve all ground users. Therefore, setting a proper value of flight altitude to balance the path loss and the coverage radius is also a key issue.

V. CONCLUSION

In this paper, we studied the problem of maximizing the minimum throughput in a RIS-assisted UAV-enabled WPCN, in which a UAV serves as a HAP to perform power transmission and data collection. The formulated optimization

problem for the joint design of the UAV's horizontal hovering location and resource allocation is non-convex due to the high degree of coupling between variables. By exploiting the SCA and SDR techniques, a low-complexity algorithm has been developed to achieve a suboptimal solution. Numerical results demonstrate that the performance of the WPCN will be substantially improved by combining UAV and RIS. In the future, dispersed but cooperative RISs and UAVs may be taken into account to expand the joint UAV's hovering location design and resource distribution scheme, which is more practical yet difficult.

APPENDIX A
PROOF OF LEMMA 1

We obtain the first-order partial derivatives of $F(m,n) = \frac{K_1}{m^\kappa} + \frac{K_2}{n^2}$ and $G(m,n) = \frac{K_3}{m^{\frac{\kappa}{2}} n}$ with respect to m and n

$$\frac{\partial F}{\partial m} = -\frac{\kappa K_1}{m^{\kappa+1}}, \frac{\partial F}{\partial n} = -\frac{2K_2}{n^3}, \\ \frac{\partial G}{\partial m} = -\frac{\frac{\kappa}{2} K_3}{m^{\frac{\kappa}{2}+1} n}, \frac{\partial G}{\partial n} = -\frac{K_3}{m^{\frac{\kappa}{2}} n}. \tag{36}$$

Then, the second-order partial derivatives of $F(m,n)$ and $G(m,n)$ are given by

$$\frac{\partial^2 F}{\partial m^2} = \frac{\kappa(\kappa+1) K_1}{m^{\kappa+2}}, \frac{\partial^2 F}{\partial n^2} = \frac{6K_2}{n^4}, \\ \frac{\partial^2 G}{\partial m^2} = \frac{\frac{\kappa}{2}\left(\frac{\kappa}{2}+1\right) K_3}{m^{\frac{\kappa}{2}+2} n}, \frac{\partial^2 G}{\partial n^2} = \frac{2K_3}{m^{\frac{\kappa}{2}} n^3}. \tag{37}$$

$$\frac{\partial^2 F}{\partial m \partial n} = \frac{\partial^2 F}{\partial n \partial m} = 0, \frac{\partial^2 G}{\partial m \partial n} = \frac{\partial^2 G}{\partial n \partial m} = \frac{\frac{\kappa}{2} K_3}{m^{\frac{\kappa}{2}+1} n^2}. \tag{38}$$

Therefore, the Hessian of $F(m,n)$ and $G(m,n)$ can be expressed as

$$\nabla^2 F = \begin{bmatrix} \frac{\partial^2 F}{\partial m^2} & \frac{\partial^2 F}{\partial m \partial n} \\ \frac{\partial^2 F}{\partial n \partial m} & \frac{\partial^2 F}{\partial n^2} \end{bmatrix}, \nabla^2 G = \begin{bmatrix} \frac{\partial^2 G}{\partial m^2} & \frac{\partial^2 G}{\partial m \partial n} \\ \frac{\partial^2 G}{\partial n \partial m} & \frac{\partial^2 G}{\partial n^2} \end{bmatrix} \tag{39}$$

Since $\frac{\partial^2 F}{\partial m^2} > 0$, $\frac{\partial^2 G}{\partial m^2} > 0$ and $\frac{\partial^2 F}{\partial m^2}\frac{\partial^2 F}{\partial n^2} - \frac{\partial^2 F}{\partial m \partial n}\frac{\partial^2 F}{\partial n \partial m} > 0$, $\frac{\partial^2 G}{\partial m^2}\frac{\partial^2 G}{\partial n^2} - \frac{\partial^2 G}{\partial m \partial n}\frac{\partial^2 G}{\partial n \partial m} = \frac{\kappa\left(\frac{\kappa}{4}+1\right) K_3^2}{m^{\kappa+2} n^4} > 0$, the Hessian matrix in (39) are positive definite. Therefore, $F(m,n)$ and $G(m,n)$ are convex function. The proof of Lemma 1 is complete. ■

REFERENCES

[1] L. Chettri and R. Bera, "A comprehensive survey on Internet of Things (IoT) toward 5G wireless systems," *IEEE Internet Things J.*, vol. 7, no. 1, pp. 16–32, Jan. 2020.
[2] G. A. Akpakwu, B. J. Silva, G. P. Hancke, and A. M. Abu-Mahfouz, "A survey on 5G networks for the Internet of Things: Communication technologies and challenges," *IEEE Access*, vol. 6, pp. 3619–3647, 2018.
[3] W. Jiang, B. Han, M. A. Habibi, and H. D. Schotten, "The road towards 6G: A comprehensive survey," *IEEE Open J. Commun. Soc.*, vol. 2, pp. 334–366, 2021.
[4] K. B. Letaief, W. Chen, Y. Shi, J. Zhang, and Y. A. Zhang, "The roadmap to 6G: AI empowered wireless networks," *IEEE Commun. Mag.*, vol. 57, no. 8, pp. 84–90, Aug. 2019.
[5] M. Di Renzo, A. Zappone, M. Debbah, M.-S. Alouini, C. Yuen, J. de Rosny, and S. Tretyakov, "Smart radio environments empowered by reconfigurable intelligent surfaces: How it works, state of research, and the road ahead," *IEEE J. Sel. Areas Commun.*, vol. 38, no. 11, pp. 2450–2525, Nov. 2020.
[6] C. You, K. Huang, H. Chae, and B.-H. Kim, "Energy-efficient resource allocation for mobile-edge computation offloading," *IEEE Trans. Wireless Commun.*, vol. 16, no. 3, pp. 1397–1411, Mar. 2017.
[7] R. Pudur, V. Hanumante, S. Shukla, and K. Kumar, "Wireless power transmission: A survey," in *Proc. Int. Conf. Recent Adv. Innov. Eng. (ICRAIE)*, May 2014, pp. 1–6.
[8] S. Bi, C. K. Ho, and R. Zhang, "Wireless powered communication: Opportunities and challenges," *IEEE Commun. Mag.*, vol. 53, no. 4, pp. 117–125, Apr. 2015.
[9] J. Hu, K. Yang, G. Wen, and L. Hanzo, "Integrated data and energy communication network: A comprehensive survey," *IEEE Commun. Surveys Tuts.*, vol. 20, no. 4, pp. 3169–3219, 4th Quart., 2018.
[10] X. Lu, P. Wang, D. Niyato, D. I. Kim, and Z. Han, "Wireless charging technologies: Fundamentals, standards, and network applications," *IEEE Commun. Surveys Tuts.*, vol. 18, no. 2, pp. 1413–1452, 2nd Quart., 2016.
[11] M. Mozaffari, W. Saad, M. Bennis, Y.-H. Nam, and M. Debbah, "A tutorial on UAVs for wireless networks: Applications, challenges, and open problems," *IEEE Commun. Surveys Tuts.*, vol. 21, no. 3, pp. 2334–2360, 3rd Quart., 2019.
[12] J. Lyu, Y. Zeng, and R. Zhang, "UAV-aided offloading for cellular hotspot," *IEEE Trans. Wireless Commun.*, vol. 17, no. 6, pp. 3988–4001, Jun. 2018.
[13] Q. Wu and R. Zhang, "Towards smart and reconfigurable environment: Intelligent reflecting surface aided wireless network," *IEEE Commun. Mag.*, vol. 58, no. 1, pp. 106–112, Nov. 2019.
[14] E. Basar, M. Di Renzo, J. De Rosny, M. Debbah, M. Alouini, and R. Zhang, "Wireless communications through reconfigurable intelligent surfaces," *IEEE Access*, vol. 7, pp. 116753–116773, 2019.
[15] Y. Liu, X. Liu, X. Mu, T. Hou, J. Xu, M. Di Renzo, and N. Al-Dhahir, "Reconfigurable intelligent surfaces: Principles and opportunities," *IEEE Commun. Surveys Tuts.*, vol. 23, no. 3, pp. 1546–1577, 3rd Quart., 2021.
[16] Z. Wei, Y. Cai, Z. Sun, D. W. K. Ng, J. Yuan, M. Zhou, and L. Sun, "Sum-rate maximization for IRS-assisted UAV OFDMA communication systems," *IEEE Trans. Wireless Commun.*, vol. 20, no. 4, pp. 2530–2550, Apr. 2021.
[17] X. Pang, M. Sheng, N. Zhao, J. Tang, D. Niyato, and K.-K. Wong, "When UAV meets IRS: Expanding air-ground networks via passive reflection," *IEEE Wireless Commun.*, vol. 28, no. 5, pp. 164–170, Oct. 2021.
[18] L. Garcia-Ordonez, A. Pages-Zamora, and J. R. Fonollosa, "Diversity and multiplexing tradeoff of spatial multiplexing MIMO systems with CSI," *IEEE Trans. Inf. Theory*, vol. 54, no. 7, pp. 2959–2975, Jul. 2008.
[19] D. Xu, Y. Sun, D. W. K. Ng, and R. Schober, "Multiuser MISO UAV communications in uncertain environments with no-fly zones: Robust trajectory and resource allocation design," *IEEE Trans. Commun.*, vol. 68, no. 5, pp. 3153–3172, May 2020.
[20] Q.-U.-A. Nadeem, A. Kammoun, A. Chaaban, M. Debbah, and M.-S. Alouini, "Asymptotic max-min SINR analysis of reconfigurable intelligent surface assisted MISO systems," *IEEE Trans. Wireless Commun.*, vol. 19, no. 12, pp. 7748–7764, Dec. 2020.
[21] L. Xie, J. Xu, and R. Zhang, "Throughput maximization for UAV-enabled wireless powered communication networks," *IEEE Internet Things J.*, vol. 6, no. 2, pp. 1690–1703, Apr. 2019.
[22] H. Chen, D. Li, Y. Wang, and F. Yin, "UAV hovering strategy based on a wirelessly powered communication network," *IEEE Access*, vol. 7, pp. 3194–3205, 2019.
[23] J. Park, H. Lee, S. Eom, and I. Lee, "UAV-aided wireless powered communication networks: Trajectory optimization and resource allocation for minimum throughput maximization," *IEEE Access*, vol. 7, pp. 134978–134991, 2019.
[24] Y. Wei, Z. Bai, and Y. Zhu, "An energy efficient cooperation design for multi-UAVs enabled wireless powered communication networks," in *Proc. IEEE 90th Veh. Technol. Conf. (VTC-Fall)*, Sep. 2019, pp. 1–5.
[25] L. Xie, J. Xu, and Y. Zeng, "Common throughput maximization for UAV-enabled interference channel with wireless powered communications," *IEEE Trans. Commun.*, vol. 68, no. 5, pp. 3197–3212, May 2020.
[26] O. S. Oubbati, M. Atiquzzaman, H. Lim, A. Rachedi, and A. Lakas, "Synchronizing UAV teams for timely data collection and energy transfer by deep reinforcement learning," *IEEE Trans. Veh. Technol.*, vol. 71, no. 6, pp. 6682–6697, Jun. 2022.
[27] Y. Zheng, S. Bi, Y. J. Zhang, Z. Quan, and H. Wang, "Intelligent reflecting surface enhanced user cooperation in wireless powered communication networks," *IEEE Wireless Commun. Lett.*, vol. 9, no. 6, pp. 901–905, Jun. 2020.

[28] B. Lyu, P. Ramezani, D. T. Hoang, S. Gong, Z. Yang, and A. Jamalipour, "Optimized energy and information relaying in self-sustainable IRS-empowered WPCN," *IEEE Trans. Commun.*, vol. 69, no. 1, pp. 619–633, Jan. 2021.
[29] Q. Wu, X. Zhou, and R. Schober, "IRS-assisted wireless powered NOMA: Do we really need different phase shifts in DL and UL?" *IEEE Wireless Commun. Lett.*, vol. 10, no. 7, pp. 1493–1497, Jul. 2021.
[30] M. Hua, Q. Wu, and H. V. Poor, "Power-efficient passive beamforming and resource allocation for IRS-aided WPCNs," *IEEE Trans. Commun.*, vol. 70, no. 5, pp. 3250–3265, May 2022.
[31] M. Hua and Q. Wu, "Joint dynamic passive beamforming and resource allocation for IRS-aided full-duplex WPCN," *IEEE Trans. Wireless Commun.*, vol. 21, no. 7, pp. 4829–4843, Jul. 2022.
[32] J. Lu, Y. Wang, Y. Chen, and H. Jia, "Joint UAV deployment and energy transmission design for throughput maximization in IoRT networks," in *Proc. IEEE/CIC Int. Conf. Commun. China (ICCC)*, Jul. 2021, pp. 236–241.
[33] J.-M. Kang, I.-M. Kim, and D. I. Kim, "Joint Tx power allocation and Rx power splitting for SWIPT system with multiple nonlinear energy harvesting circuits," *IEEE Wireless Commun. Lett.*, vol. 8, no. 1, pp. 53–56, Feb. 2019.
[34] H. Xie, J. Xu, and Y.-F. Liu, "Max-min fairness in IRS-aided multi-cell MISO systems with joint transmit and reflective beamforming," *IEEE Trans. Wireless Commun.*, vol. 20, no. 2, pp. 1379–1393, Feb. 2021.
[35] A. Alkhateeb and R. W. Heath, "Frequency selective hybrid precoding for limited feedback millimeter wave systems," *IEEE Trans. Commun.*, vol. 64, no. 5, pp. 1801–1818, May 2016.
[36] Y. Zeng, Q. Wu, and R. Zhang, "Accessing from the sky: A tutorial on UAV communications for 5G and beyond," *Proc. IEEE*, vol. 107, no. 12, pp. 2327–2375, Dec. 2019.
[37] A. Goldsmith, *Wireless Communications*. Cambridge, U.K.: Cambridge Univ. Press, 2005.
[38] X. Shen, S. Diamond, Y. Gu, and S. Boyd, "Disciplined convex-concave programming," in *Proc. IEEE 55th Conf. Decis. Control (CDC)*, Dec. 2016, pp. 1009–1014.
[39] *MOSEK Optimization Toolbox for MATLAB. User's Guide and Reference Manual*, document Version 4.1, Mosek ApS, Denmark, U.K., 2019.
[40] M. Grant and S. Boyd. (2014). *CVX: MATLAB Software for Disciplined Convex Programming, Version 2.1*.[Online]. Available: http://cvxr.com/cvx/
[41] Q. Wu and R. Zhang, "Intelligent reflecting surface enhanced wireless network via joint active and passive beamforming," *IEEE Trans. Wireless Commun.*, vol. 18, no. 11, pp. 5394–5409, Nov. 2019.
[42] S. Li, B. Duo, X. Yuan, Y.-C. Liang, and M. Di Renzo, "Reconfigurable intelligent surface assisted UAV communication: Joint trajectory design and passive beamforming," *IEEE Wireless Commun. Lett.*, vol. 9, no. 5, pp. 716–720, Jan. 2020.

JIAYING ZHANG received the B.Eng. degree from the College of Electronic Science and Engineering, Jilin University, Changchun, China, in 2021. She is currently pursuing the M.Sc. degree with the School of Electronic and Information Engineering, South China University of Technology, China, under the supervision of Prof. Jie Tang and Prof. Xiu Yin Zhang. Her research interests include wireless information and power transfer, reconfigurable intelligent surface, energy efficiency optimization, and 5G/6G networks.

JIE TANG (Senior Member, IEEE) received the B.Eng. degree from the South China University of Technology, China, the M.Sc. degree from the University of Bristol, U.K., and the Ph.D. degree from Loughborough University, U.K.

From 2013 to 2015, he was a Research Associate with the School of Electrical and Electronic Engineering, The University of Manchester, U.K. He is currently a Professor with the School of Electronic and Information Engineering, South China University of Technology, China. His current research interests include SWIPT , UAV communications, NOMA, and reconfigurable intelligent surface. He received the IEEE ComSoc Asia–Pacific Outstanding Young Researcher Award in 2021. He was a co-recipient of the Best Paper Awards from ICNC 2018, CSPS 2018, WCSP 2019, 6GN 2020, and AICON2021. He served as the Track Co-Chair for IEEE VTC-Spring 2018 and 2022, the Symposium Co-Chair for IEEE/CIC ICCC 2020 and IEEE ComComAp 2019, the TPC Co-Chair for EAI GreeNets 2019, and the Workshop Co-Chair for IEEE ICCC/CIC 2019. He is the current Vice Chair of the Special Interest Group on Green Cellular Networks within the IEEE ComSoc Green Communications and Computing Technical Committee. He is also serving as an Editor for IEEE Wireless Communications Letters, IEEE Systems Journal, and *EURASIP Journal on Wireless Communications and Networking*. He is the Guest Editor for two special issues on IEEE Transactions on Green Communications and Networking, and one special issue on IEEE Open Journal of the Communications Society.

WANMEI FENG received the M.Sc. degree from the Department of Physics and Telecommunications Engineering, South China Normal University (SCNU), Guangzhou, China, in 2018, and the Ph.D. degree from the School of Electronic and Information Engineering, South China University of Technology, China, in 2022. She is currently an Associated Professor with the College of Electronic Engineering (College of Artificial Intelligent), South China Agricultural University, Guangzhou. Her research interests include energy efficiency optimization, integrated sensing and communications, UAV communications, non-orthogonal multiple access, simultaneous wireless information, and power transfer and 6G networks.

XIU YIN ZHANG received the B.S. degree in communication engineering from the Chongqing University of Posts and Telecommunications, Chongqing, China, in 2001, the M.S. degree in electronic engineering from the South China University of Technology, Guangzhou, China, in 2006, and the Ph.D. degree in electronic engineering from the City University of Hong Kong, Hong Kong, SAR, China, in 2009. From 2001 to 2003, he was with ZTE Corporation, Shenzhen, China. From July 2006 to June 2007, he was a Research Assistant with the City University of Hong Kong, where he was a Research Fellow, from September 2009 to February 2010. He is currently a Full Professor and the Vice Dean of the School of Electronic and Information Engineering, South China University of Technology. He is also the Director of the Engineering Research Center for Short-Distance Wireless Communications and Network, Ministry of Education. He has authored or coauthored more than 180 internationally refereed journal articles (including more than 100 IEEE Transactions) and 90 conference papers. His research interests include antennas, MMIC, RF components and sub-systems, and intelligent wireless communications and sensing. He is a fellow of the Institution of Engineering and Technology (IET). He was a recipient of the National Science Foundation for Distinguished Young Scholars of China. He won the First Prize of the 2015 Guangdong Provincial Natural Science Award and the 2020 Guangdong Provincial Technological Invention Award. He served as the general chair/the co-chair/the technical program committee (TPC) chair/a member, a session organizer/the chair for a number of conferences. He was a supervisor of several conference best paper award winners. He is an Associate Editor of IEEE Antennas and Wireless Propagation Letters, *IEEE Antennas and Propagation Magazine*, and IEEE Open Journal of Antennas and Propagation.

DANIEL KA CHUN SO (Senior Member, IEEE) received the B.Eng. degree (Hons.) in electrical and electronics engineering from the University of Auckland, New Zealand, and the Ph.D. degree in electrical and electronics engineering from The Hong Kong University of Science and Technology (HKUST).

He joined The University of Manchester, as a Lecturer, in 2003. He is currently a Professor and the Discipline Head of Education of the Department of Electrical and Electronic Engineering, University of Manchester. His research interests include green communications, NOMA, beyond 5G and 6G networks, machine learning and federated learning, heterogeneous networks, SWIPT, massive MIMO, cognitive radio, and D2D and cooperative communications. He served as the Symposium Co-Chair for IEEE ICC 2019 and Globecom 2020 and the Track Co-Chair for the IEEE Vehicular Technology Conference (VTC) Spring 2016, 2017, 2018, 2021, and 2022, and VTC Fall 2023. He has been the Chair of the Special Interest Group on Green Cellular Networks within the IEEE ComSoc Green Communications and Computing Technical Committee, since 2020. He is also serving as a Senior Editor for IEEE Wireless Communications Letters after being an Editor from 2016 to 2020 and an Editor for IEEE Transactions on Wireless Communications. He is the Lead Guest Editor for a Special Issue on IEEE Transactions on Green Communications and Networking, in 2021.

KAT-KIT WONG received the B.Eng., M.Phil., and Ph.D. degrees in electrical and electronic engineering from The Hong Kong University of Science and Technology, Hong Kong, in 1996, 1998, and 2001, respectively. After graduation, he took up academic and research positions with The University of Hong Kong; Lucent Technologies; Bell-Labs; Holmdel; Smart Antennas Research Group, Stanford University; and the University of Hull, U.K. He is currently the Chair of the Wireless Communications, Department of Electronic and Electrical Engineering, University College London, U.K. His current research interests include 5G and beyond mobile communications. He is fellow of IET. He was a co-recipient of the 2013 IEEE Signal Processing Letters Best Paper Award and the 2000 IEEE VTS Japan Chapter Award at the IEEE Vehicular Technology Conference, Japan, in 2000, and a few other international best paper awards. He is also on the editorial board of several international journals. He is the Editor-in-Chief of IEEE Wireless Communications Letters, since 2020.

JONATHON A. CHAMBERS (Fellow, IEEE) received the Ph.D. and D.Sc. degrees in signal processing from the Imperial College of Science, Technology and Medicine (Imperial College London), London, U.K., in 1990 and 2014, respectively.

In 2015, he joined the School of Electrical and Electronic Engineering, Newcastle University, where he was a Professor of signal and information processing and led the Intelligent Sensing and Communications Group and is currently a Visiting Professor. He is an Emeritus Professor and was the former Head of the Engineering, University of Leicester, from 2017 to 2019. He has advised approaching 100 researchers through to Ph.D. graduation and authored or coauthored more than 600 conference papers and journal articles, many of which are in IEEE journals. His research interests include adaptive signal processing and machine learning and their applications.

Dr. Chambers is a fellow of the Royal Academy of Engineering, U.K., and the Institution of Electrical Engineers. He was a member of the IEEE Signal Processing Conference Board and the European Signal Processing Society Best Paper Awards Selection Panel. He was the Technical Program Chair of the 15th International Conference on Digital Signal Processing and the 2009 IEEE Workshop on Statistical Signal Processing, both held in Cardiff, U.K., and the Technical Program Co-Chair of the 36th IEEE International Conference on Acoustics, Speech, and Signal Processing, Prague, Czech Republic. He served on the IEEE Signal Processing Theory and Methods Technical Committee for six years and the IEEE Signal Processing Society Awards Board for three years. He additionally served as an Associate Editor for IEEE Transactions on Signal Processing for three terms over the periods 1997–1999 and 2004–2007 and as a Senior Area Editor from 2011 to 2014.